Geol. Mag. **156** (*3*), *2019, pp. 510–524* © *Cambridge University Press 2017*
doi:10.1017/S0016756817000966

Eocene magmatism from the Liemai intrusion in the Eastern Tethyan Himalayan Belt and tectonic implications

LIMING TIAN*, LIYUAN WANG‡†, HAITAO ZHENG§ & BO YANG¶

*Geophysical and Geochemical Exploration Brigade of Jiangxi, Nanchang, 330002, China
‡College of Zijin Mining, Fuzhou University, Fuzhou, 350116, China
§Institute of Geological Survey, China University of Geosciences, Wuhan, 430074, China
¶College of Energy, Chengdu University of Technology, Chengdu, China

(*Received* 27 February 2017; *accepted* 19 October 2017; *first published online* 27 November 2017)

Abstract – Multistage magmatic thermal events occurred in the Yardoi Dome and contain important information on the tectonomagmatic processes. The dome has played a crucial role in understanding the collisional evolution of the Tethyan Himalayan. We present new geochronological and geochemical data for muscovite-granite exposed in the Liemai area, Eastern Tethyan Himalayan Belt. Liemai muscovite-granite is strongly peraluminous, with A/CNK values characterized by evolved geochemical composition with high contents of SiO_2-enriched large-ion lithophile elements, and is depleted of high-field-strength elements. These geochemical features indicate that granites possibly derived from partial melting of metasedimentary rocks and plagioclase fractional crystallization probably played a critical role in production of peraluminous granitic melts. Zircon U–Pb dating from muscovite-granite yielded ages of approximately 48.5 ± 1.1 Ma, representing its crystallization ages. This age is the oldest age of Tethyan Himalayan leucogranite from the Yardoi Dome and adjacent areas. However, the inherited zircon cores have ages of 135.7–3339.2 Ma. The εHf(t) values of all zircons vary from –6.4 to –2.3 and have varying Hf-isotope crustal model ages of 731–839 Ma. The geochemical and isotopic compositions indicate that magma of the Liemai granite can most likely be interpreted as products of the break-off related to thermal perturbation along the break-off window associated with the subduction of Neo-Tethyan slab. These magmas were derived mainly from the anatexis of ancient crustal materials under contraction and thickening conditions due to subduction of the Indian continent beneath southeastern Tibet.

Keywords: Tethyan Himalaya, Liemai muscovite-granite, Zircon U–Pb dating, crustal anatexis

1. Introduction

The India–Eurasia continent–continent collision may be divided into three stages: main collision (41–65 Ma), later collision (26–40 Ma) and post-collision (0–25 Ma) (Ding *et al.* 2003; Mo *et al.* 2003; Hou *et al.* 2006). Intensive crustal anatexis of the Himalayan Orogenic Belt led to the formation of two subparallel leucogranitic belts separated by the southern Tibetan detachment system (STDS): the High Himalayan Gneiss Dome (NHGD) in the south and North Himalayan Gneiss Dome (NHGD) in the north (Fig. 1a). These leucogranites are important 'lithoprobes' and 'windows' for investigating the tectonomagmatic evolution history of the Himalayan Orogenic Belt (Mo *et al.* 2003; Liao *et al.* 2007) and for understanding crustal thickening, anatexis and plateau uplift during continental collisions (Zhang *et al.* 2004, 2012; Zeng *et al.* 2009; Xie *et al.* 2010). Cenozoic magmatism in the Himalayas produced mainly Oligocene–Miocene leucogranites that occur in in two subparallel belts in the Tethyan and High Himalayas (Wu *et al.* 2015), along with minor middle Eocene (42–46 Ma) granites in the Tethyan Himalaya. The leucogranites mainly intruded in the central part of the Tethyan Himalaya Metamorphic Domes, such as the Lhagoi, Kangmar and Yardoi domes. A small proportion of the leucogranites occur as individual intrusions or dykes intruded into the Tethyan Himalaya low-grade metamorphic rocks, such as Changguo, Qiazuweng, Peikucuo, Zharizhongshi and Xiaru in the west and Dala and Quedang in the east (Fig. 1a).

The Yardoi Dome is one such important window for studying collisional orogeny and deep processes in the Tethyan Himalaya Tectonic Belt (Wu *et al.* 2014). Studies of the formation and evolution of the Yardoi Dome reveal at least three partial melting events. The first event corresponds to the main stage of collision, as represented by the formation of two-mica granites with crystallization ages of 43–45 Ma (Aikman, Harrison & Lin, 2008; Qi *et al.* 2008; Zeng *et al.* 2011; Wu *et al.* 2014) and associated subvolcanic rocks with a crystallization age of 40.9 Ma (Hu *et al.* 2011). The second event was recorded by the intrusion of leucogranitic dykes at *c.* 35 Ma, which induced activity along the southern Tibetan detachment system (STDS) (Gao *et al.* 2009; Zeng *et al.* 2009; Wu *et al.* 2014). The third event was represented by the formation of

†Author for correspondence: Email: wangliyuan030101@163.com

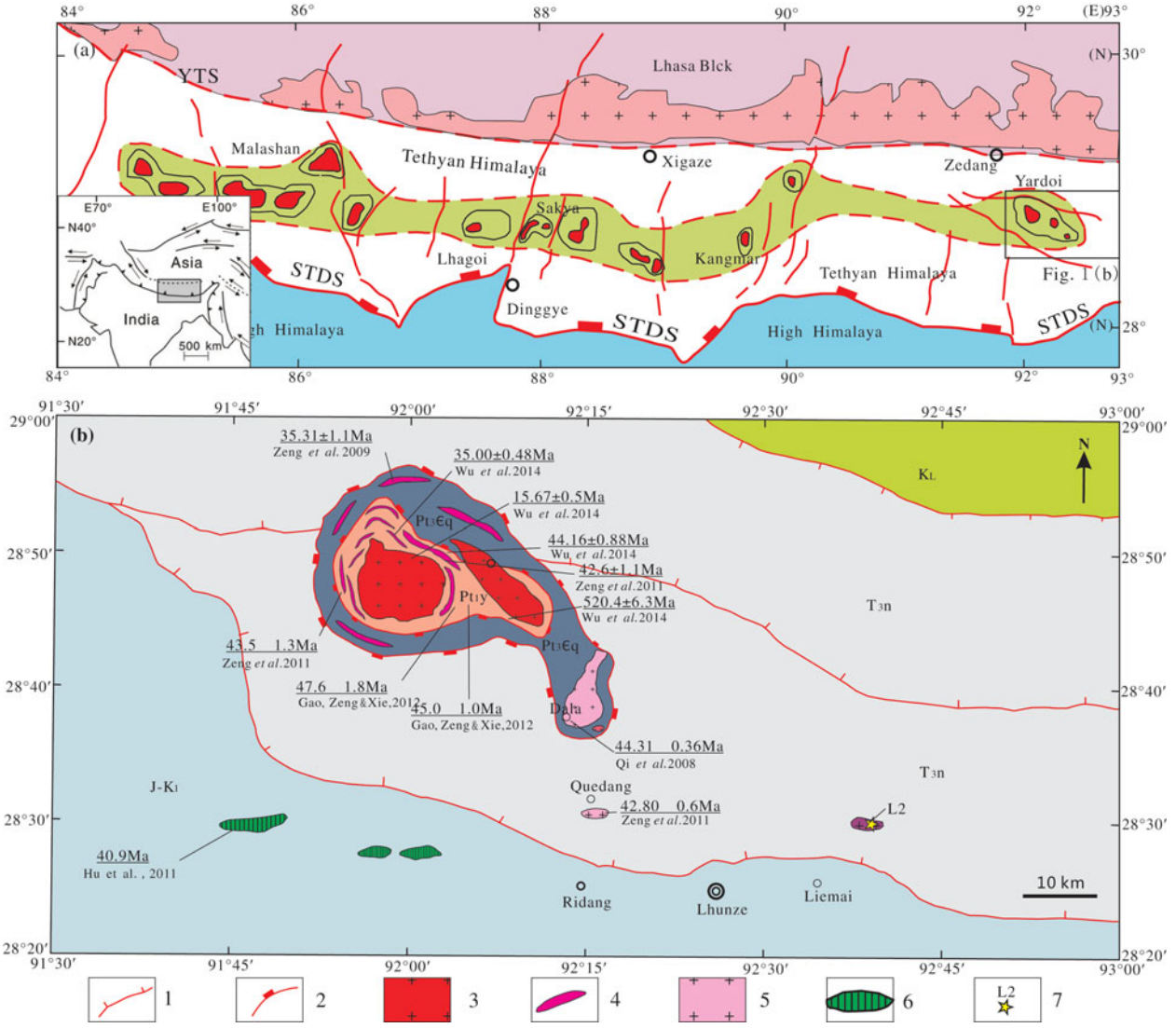

Figure 1. (Colour online) Simplified geological map of (a) the Himalayan Orogenic Belt, southern Tibet (Zeng *et al.* 2011) and (b) simplified geological map of the Yardoi area showing the Yardoi gneiss dome (recompiled from 1:250 000 Longzi regional geological map). 1, thrust fault; 2, detachment fault; 3, early–middle Miocene leucogranites; 4, Eocene two-mica granite dykes; 5, early Eocene leucogranites granite; 6, rhyolitic subvolcanic rock; 7, sampling position and number. J–K_1 – Lower Cretaceous – Triassic limestone, sandstone, conglomerate; T_3n – Upper Triassic sandstone and slate of Langxuejie Group, Nieru Formation; K_L – Cretaceous tectonic complex; $Pt_3Єq$ – schist in Qudegong Formation; Pt_1y – gneiss and amphibolite in Yatuizhala Formation.

large-scale leucogranite intrusions in the central Yardoi Dome at *c.* 15 Ma (Wu *et al.* 2014). The metamorphic ages of gneiss and garnet amphibolite within the Yardoi Dome are 47.6 Ma and 43.5–45.0 Ma, respectively (Zeng *et al.* 2011; Gao, Zeng & Xie, 2012).

Currently, the tectonic setting and origin of the Tethyan Himalaya leucogranites is controversial. Some researchers have proposed a mechanism of partial melting of the metasedimentary rocks of the high Himalayan crystalline rock series to create the leucogranites (Harris & Inger, 1992; Harrison *et al.* 1999; Guo & Li, 2007; Huang *et al.* 2013). Others have argued that leucogranites originated primarily from amphibolite-dehydrated melting and secondly from metapelite partial melting under crustal thickening conditions (Gao *et al.* 2009; Zeng *et al.* 2009, 2011; Gao, Zeng & Hu, 2010; Xie *et al.* 2010; Gao, Zeng & Xie, 2012). Nevertheless, the crystallization age of the leucogranite is apparently younger than the metamorphic age of the para-metamorphic gneiss. With higher temperatures and slower cooling within the metamorphic dome, melt crystallization may lag behind partial melting, giving rise to a younger leucogranite crystallization age than metamorphic age. Whereas magma intruded into the upper cooler sedimentary rocks, crystallization occurred rapidly and its crystallization age is a better representation of the age of partial melting. Understanding the leucogranite that intruded into the Tethyan Himalaya low-grade metamorphic rocks is therefore important to constrain the age of partial melting and the relationship with metamorphism and deep processes (Wu *et al.* 2015).

New SHRIMP zircon U–Pb data imply that multiphased magmatic thermal events and intense ductile

https://doi.org/10.1017/S0016756817000966 Published online by Cambridge University Press

shearing occurred in the Yardoi Dome of the Eastern Tethyan Himalaya Belt, which recorded the structural deformation and thermal history caused by northwards subduction of the Indian Continental Plate (Qi *et al.* 2008; Zeng *et al.* 2012; Wu *et al.* 2014). The Yardoi Dome is therefore a key area for understanding the geological tectonic-thermal events that occurred during the Cenozoic collisional orogeny.

In this contribution, we present new field-based geological, geochemical and laser ablation inductively coupled plasma mass spectrometry (LA-ICP-MS) U–Pb zircon age data for the Liemai muscovite-granite of the Yardoi Dome. We discuss new evidence of the ages, petrogeochemistry, source region features, tectonic environment and formation mechanisms. This contribution provides insights into the petrogenesis of these granites and provides new constraints on the Eocene tectonic evolution of the Tethyan Himalaya leucogranite.

2. Geological background and sample descriptions

The Yardoi Dome is located at the easternmost end of the Tethyan Himalaya Orogenic Belt (Fig. 1a) and consists of: leucogranitic sill and sheared muscovite-granite in the core; and three litho-tectonic units separated by two detachment faults of high-graded garnet-bearing metapelite, amphibolite and graphite schist in the margin. Leucogranite dykes intruded into the garnet graphite schist and gneiss in the margin and rim of this dome (Zeng *et al.* 2011). Previous studies divided the supracrustal rock sequences of the Yardoi Dome into three major units, including: (1) high-grade metamorphic rock units in the core; (2) intermediate-grade metamorphic rock units in the middle; and (3) sedimentary rocks and intrusive granites along the margin. These rock units are separated by ductile or brittle-ductile detachment faults (Zhang, Guo & Zhang, 2007) (Fig. 1b). The margin of the Yardoi Dome consists of upper Permian or Upper Triassic Tethys marine clastic sedimentary rocks, accompanied by mafic dykes composed of diabase, sillite and leucogranite.

High-resolution zircon dating indicated four periods of tectonic magmatic events that took place in the Yardoi Dome. The ancient age of the zircon (*c.* 520.4–536 Ma) revealed the magmatic emplacement of the Pan-African Orogeny in the crystalline basement of the Himalayan block. The other isotopic ages of the zircons revealed tectonic-thermal events during the Cenozoic collisional orogeny. The inner core of Yardoi Dome comprises a two-mica granite pluton with a crystallization age of *c.* 43–45 Ma, indicative of the initial time of the northwards subduction of the Indian Continental Plate. Zircons aged *c.* 35 Ma may represent partial melting of dominantly garnet amphibolites under thickened crustal conditions, and those of age *c.* 15 Ma represent the epoch of the emplacement of the core granite and the formation of the Yardoi Dome (Wu *et al.* 2014).

The Liemai pluton is located within the Tethyan Himalaya Belt, SE of the Yardoi Dome. The Liemai muscovite-granite is located north of Yu village, Liemai town, Lhunze county, with geographic coordinates of 92° 40′ E, 28° 27′ N. It is approximately 25 km from Lhunze county. The Liemai leucogranite has a N–S width of 500 m. The Liemai pluton is intruded into sandstone and slate of the Tethyan sedimentary sequence to the SE of the Yardoi Dome. Some intensely deformed dykes, varying in width from several centimetres to metres, intrude into the Triassic metasedimentary rocks in this region. The country rocks are fine-grained, medium- to thick-bedded metamorphic quartz sandstones of the Langjiexue Group Nieru Formation (T_3n), intercalated with dark-grey silty sericite slates (Fig. 1b). Detailed field investigations indicate that the pelitic sediments were intruded by the leucogranites and also the presence of metamorphism, with grade increasing towards the granite core. The lack of sillimanite or migmatite in the metasedimentary wall-rocks implies relatively lower metamorphic grade. A suite of muscovite-granites from Liemai was collected for petrological, geochemical and geochronological studies. The muscovite-granite shares the same porphyritic texture and comprises phenocrysts of plagioclase (5 %), muscovite (5 %) and quartz (1 %) (Fig. 2). The plagioclase phenocrysts have an euhedral tabular shape with sericitization. Quartz occurs as anhedral granular aggregates, whereas the muscovite phenocrysts occur as subhedral flakes. The matrix has a fine-grained granitic texture, consisting mainly of quartz (*c.* 45 %), muscovite (*c.* 20 %), K-feldspar (*c.* 15 %) and plagioclase (*c.* 10 %).

3. Analytical methods

3.a. Major- and trace-element geochemistry

Whole-rock major- and trace-element compositions (Table 1) were determined at the Ministry of Land and Resources (MLR) Wuhan Mineral Resources Supervision and Test Center. Rock samples were carefully selected and sawed into slabs. The central parts were crushed and ground to finer than 200 mesh (*c.* 80 μm) for the bulk-rock analyses. The major components of these samples were analysed using an automatic X-ray fluorescence (XRF) spectrometer, Thermo ArlAdvant XP+. Sample powders were made into glass disks after fusion with lithium metaborate. Samples and flux materials were mixed at a 1:10 ratio and fused at 1100 °C in a Pt-Au crucible for 20–40 min. Trace elements, including rare Earth and refractory elements, were analysed using an XSeries II ICP mass spectrometer. Loss on ignition (LOI) values were obtained by using an electronic analytical balance after ignition at 1000 °C. The analytical precisions for all major-element abundances were better than 2–3 wt %. The analytical uncertainties for the trace elements were 10 % (for those with abundances of less than 10 ppm) and *c.* 5 % (for those with concentrations of more than 10 ppm)

https://doi.org/10.1017/S0016756817000966 Published online by Cambridge University Press

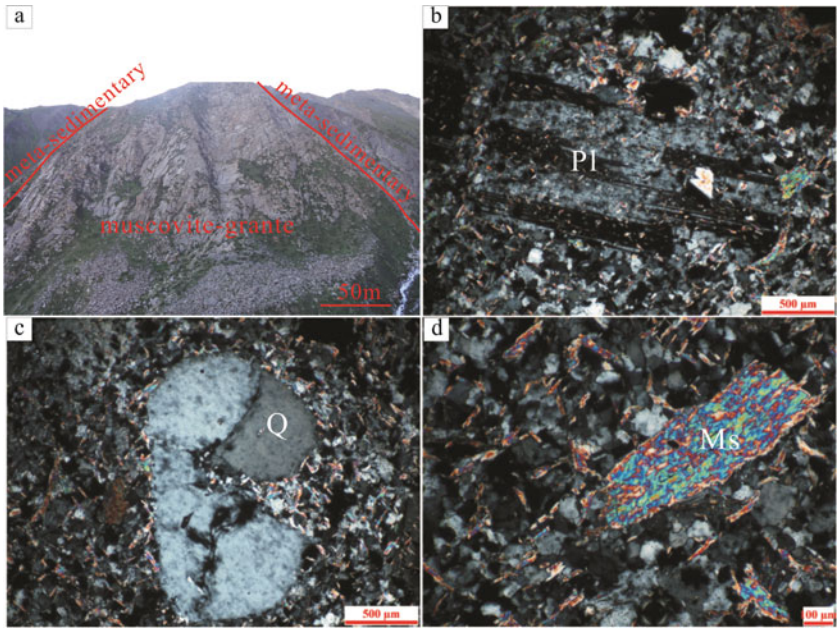

Figure 2. (Colour online) Photograph and micrographs of muscovite-granite from Liemai. (a) Field characters of Liemai leucogranite (lens to the west). Phenocrysts of (b) plagioclase, (c) quartz and (d) muscovite. Ms –muscovite; Pl – plagioclase; Q – quartz.

3.b. Zircon U–Pb dating

Separation of zircon crystals was completed in the laboratory of the Hebei Institute of Regional Geological Survey. Leucogranite samples were first crushed and then gravity sorted. Transparent, colourless, crackless and well-crystallized zircon grains were hand-picked under a binocular microscope. The crystals were then mounted on epoxy discs and polished to reveal their internal growth textures and morphology, followed by examination using cathodoluminescence (CL) imaging and scanning electron microscope (SEM). U–Pb dating was conducted on selected zircon crystals using a LA-MC-ICP-MS at the State Key Laboratory of Geological Processes and Mineral Resources (GPMR) at the China University of Geosciences. The diameter of the laser beam was 32 μm, and the spot ablation depth was 20–40 μm. The Harvard University 91500 zircon was chosen as the correction standard. Detailed analytical data showing individual analyses with a 1σ error are listed in Table 2. The resultant data were processed offline using the ICP-MS Data Cal 4.3 program (Liu *et al.* 2010). The age calculation and the plotting of concordia diagrams were performed using Isoplot 4.0.

3.c. Zircon Hf isotopic composition

Hf isotopic analyses were performed on the same spots or age domains as the age determinations of the concordant grains, based on the CL images after the U–Pb isotopic analyses. The *in situ* zircon Hf isotope measurements were performed on a LA-MC-ICP-MS in the GPMR. The beam size was 44 μm. The standard sample and data processing software were the same as used for zircon U–Pb dating. Details of the Hf isotopic analytical method are given by Hu *et al.* (2012). Each measurement comprised a 10 s pre-ablation, a 45 s ablation and a 30 s washout delay. The isobaric interference of ^{176}Lu and ^{176}Yb on ^{176}Hf was corrected by monitoring the signal intensity of ^{175}Lu, ^{173}Yb and ^{172}Yb of the individual spot.

4. Results

4.a. Whole-rock geochemical compositions

Whole-rock major- and trace-element data are provided in online Supplementary Table S1 (available at http://journals.cambridge.org/geo). The Liemai muscovite-granites are relatively enriched in silicon and aluminium (SiO_2 = 70.45–72.08 %; Al_2O_3 = 15.42–16.26 %), but are depleted in magnesium and calcium (MgO < 0.6 %, CaO = 0.2–1.12 %). All samples are plotted in the area of high-K calc-alkaline series (Fig. 3a). The Liemai granite is peraluminous, as suggested by the presence of certain minerals (e.g. muscovite, A/CNK>1.1 and corundum in its CIPW norm) (Fig. 3b). These features show that the Leimai granite is an S-type granite that was possibly derived from partial melting of metasedimentary rocks. The Liemai muscovite-granites are therefore high-K calc-alkaline peraluminous in nature, different from granites from the middle and core parts of the Dala, Quedang and Yardoi domes where the latter have a lower CaO content and CaO/Na_2O ratios (<0.3) but higher K_2O/Na_2O ratios (>1.0).

On the primitive-mantle-normalized multi-element spider diagrams (Fig. 4a), samples from the Liemai muscovite-granites appear as right-sloping multiple-peak-valley patterns, similar to the two-mica granites of the Dala, Quedang and Yardoi domes. However,

https://doi.org/10.1017/S0016756817000966 Published online by Cambridge University Press

Table 1. Whole-rock major- (wt %) and trace-element ($\times 10^{-6}$) compositions of Liemai granites

Sample	LM1	LM2	LM3	LM4	LM5	LM6	LM7	LM8	LM9	LM10
					Major element (wt %)					
SiO_2	70.87	71.34	70.45	72.08	71.18	71.98	71.08	71.21	71.1	71.49
TiO_2	0.19	0.23	0.18	0.32	0.18	0.25	0.21	0.21	0.21	0.21
Al_2O_3	16.08	15.7	15.42	16.5	15.58	16.26	15.58	15.6	15.72	15.55
Fe_2O_3	0.2	0.36	0.58	0.56	0.56	0.55	0.33	0.32	0.36	0.41
FeO	0.97	1.18	1.33	1.18	0.17	0.25	1.08	1.1	1.13	1.03
MnO	0.03	0.01	0.02	0.01	0.01	0.005	0.02	0.02	0.03	0.02
MgO	0.23	0.24	0.2	0.24	0.19	0.24	0.55	0.59	0.58	0.56
CaO	1.09	0.85	0.23	0.2	0.24	0.21	0.92	1.12	0.88	0.89
Na_2O	3.78	3.86	3.14	3.95	4.71	2.98	3.92	3.96	3.93	3.92
K_2O	3.9	4.75	4.39	2.92	4.62	3.35	4.47	4.32	4.53	4.57
P_2O_5	0.13	0.09	0.28	0.09	0.25	0.08	0.12	0.11	0.11	0.11
LOI	0.78	1.76	0.62	1.38	1.52	0.93	1.50	0.98	1.05	0.96
TOTAL	100.42	101.95	99.09	101.02	99.02	99.04	99.81	99.59	99.74	99.8
A/CNK	1.30	1.20	1.49	1.65	1.18	1.83	1.20	1.18	1.21	1.20
					Trace element (ppm)					
Sc	1.35	1.34	1.25	1.49	1.28	1.27	2.9	2.81	3.01	2.76
V	4.38	4.52	4.35	4.23	3.99	4.16	19.61	18.78	19.26	18.59
Cr	2.99	3.37	3.81	3.56	3.29	3.35	8.61	11.45	12.14	12.65
Co	0.59	0.44	0.62	0.53	0.52	0.6	2.45	2.95	5.35	2.89
Ni	1.52	1.71	1.9	2.14	2.14	2.74	9.79	9.66	11.69	9.66
Rb	229	198.8	186	221.7	166.6	248.9	293.8	288.3	213.4	204.1
Sr	44.6	50.3	53.1	60.3	119.8	53.3	133.6	131.6	131.7	134.5
Zr	49.6	53	50.4	52.8	52.3	51.1	74.7	82.1	80.8	78.4
Nb	5.03	5.31	5.75	5.21	4.98	4.96	6.05	5.43	5.19	5.5
Ba	255.5	284.5	233.9	325.6	203.8	293.3	217.1	264.6	289.2	261.5
Hf	3.16	2.32	1.93	2.32	3.48	3.27	3.3	3.15	3.42	3.53
Ta	0.9	0.89	1.12	0.89	0.88	0.87	0.88	0.69	0.66	0.69
U	2.34	1.98	2.69	2.13	2.85	2.34	2.14	2.83	1.96	2.75
Th	10.54	9.34	10.98	9.96	11.67	10.67	11.6	10.5	9.8	11.5
Li	889.4	1130	738	803.4	29.14	401.5	253.9	389.5	310.2	314.7
Be	8.53	9.34	10.01	9.79	15.88	11.53	15.82	15.21	10.12	15.83
Cs	29.19	23.42	22.26	30.83	22.03	38.94	19	18.9	16.83	17.86
La	17.32	18.8	16.87	18.28	18.32	18.37	24.24	24.55	25.12	24.49
Ce	34.9	37.98	33.84	36.8	37.03	36.93	47.35	48.73	50.46	48.65
Pr	4.05	4.36	3.92	4.22	4.3	4.31	5.55	5.73	5.8	5.78
Nd	14.01	15.43	13.53	14.7	15.01	15.17	19.37	19.7	20.38	20.07
Sm	3.14	3.87	3.4	3.59	3.88	3.86	4.4	4.39	4.55	4.42
Eu	0.67	0.78	0.64	0.71	0.94	0.8	1.02	1.02	1.07	1.03
Gd	2.06	3.02	2.58	2.73	2.92	2.92	3.31	3.3	3.47	3.26
Tb	0.22	0.34	0.3	0.31	0.33	0.31	0.37	0.35	0.37	0.37
Dy	0.77	1.25	1.05	1.11	1.07	1.08	1.47	1.33	1.38	1.36
Ho	0.1	0.15	0.13	0.14	0.13	0.12	0.2	0.17	0.19	0.18
Er	0.2	0.28	0.25	0.24	0.23	0.23	0.42	0.36	0.37	0.37
Tm	0.02	0.03	0.03	0.03	0.03	0.03	0.05	0.04	0.04	0.04
Yb	0.13	0.18	0.15	0.15	0.15	0.14	0.29	0.23	0.24	0.22
Lu	0.02	0.02	0.02	0.02	0.02	0.02	0.04	0.03	0.03	0.03
Y	2.63	3.91	3.44	3.64	3.24	3.52	5.58	4.8	5.04	4.85
δEu	0.76	0.67	0.63	0.67	0.82	0.70	0.78	0.79	0.79	0.79

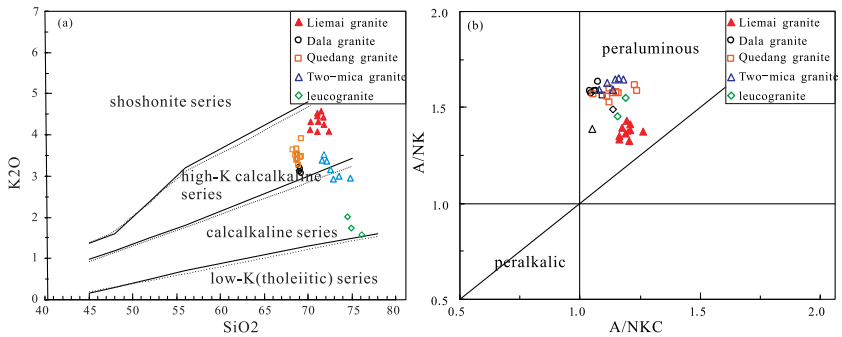

Figure 3. (Colour online) (a) K_2O–SiO_2 and (b) A/NK-A/CNK diagrams for typical granites from the Yardoi area (data sources: Dala granite from Xie *et al.* 2010; Quedang granite from Gao, Zeng & Hu, 2010; two-mica granite and leucogranite from Gao *et al.* 2009).

https://doi.org/10.1017/S0016756817000966 Published online by Cambridge University Press

Table 2. U–Th–Pb composition of zircons from Liemai granite measured by LA-ICP-MS

Sample no.	U ($\times10^{-6}$)	Th ($\times10^{-6}$)	Pb ($\times10^{-6}$)	Th/U	Isotope ratio						Note	$^{207}Pb/^{206}Pb$ age (Ma)	1σ	$^{207}Pb/^{235}U$ age (Ma)	1σ no.	$^{206}Pb/^{238}U$ ($\times10^{-6}$)	1σ
					$^{207}Pb/^{206}Pb$	σ (%)	$^{207}Pb/^{235}U$	σ (%)	$^{206}Pb/^{238}U$	σ (%)							
LM2-1	291	343	103	1.18	0.0588	0.004	0.68686	0.044	0.08469	0.002	core	560.9	76.5	530.9	26.3	524	12
LM2-2	11466	485	313.8	0.04	0.0469	0.003	0.0467	0.002	0.00723	0.0002	rim	42.8	79.2	46.3	2.3	46.5	1.3
LM2-3	202	51	17.8	0.25	0.0547	0.005	0.16593	0.015	0.022	0.0005	core	399.4	112.8	155.9	12.7	140.3	3.2
LM2-4	2673	26	7.6	0.01	0.0588	0.008	0.05802	0.007	0.00716	0.0002	rim	559.4	156.7	57.3	6.6	46	1.2
LM2-5	106	73	29.8	0.69	0.0777	0.006	0.73009	0.058	0.0681	0.0018	core	1140	85.6	556.6	34	424.7	11.1
LM2-6	2389	195	69.3	0.08	0.051	0.003	0.0509	0.003	0.00723	0.0001	rim	241.8	74.1	50.4	2.7	46.5	0.8
LM2-7	143	72	19	0.5	0.0554	0.004	0.25264	0.017	0.03306	0.0007	core	428.8	89.2	228.7	14	209.7	4.2
LM2-8	166	100	373.8	0.6	0.276	0.013	20.312	1.065	0.534	0.012	core	3339.2	40.2	3106.3	50.8	2758.3	49.5
LM2-9	422	101	151.8	0.24	0.0624	0.004	0.77229	0.051	0.08972	0.0018	core	1035.6	59.9	665.7	24.9	553.9	10.5
LM2-10	296	213	190.2	0.72	0.0739	0.003	1.5771	0.078	0.15475	0.0032	core	1038.4	50.8	961.2	30.6	927.5	17.7
LM2-11	314	100	651.9	0.32	0.0697	0.003	1.15884	0.058	0.12062	0.0022	core	917.9	52.2	781.4	27.2	734.1	12.7
LM2-12	429	366	325.8	0.85	0.0875	0.004	2.20789	0.112	0.18297	0.0039	core	1371.2	51	1183.5	35.6	1083.2	21
LM2-13	190	55	16.8	0.29	0.0494	0.004	0.14831	0.012	0.02176	0.0005	core	168.5	107.8	140.4	10.5	138.7	2.8
LM2-14	10181	913	662.6	0.09	0.0648	0.051	0.0695	0.054	0.00778	0.0004	rim	4134.2	50.5	723.3	31.7	50	2.3
LM2-15	70	114	24.6	1.63	0.0528	0.004	0.62641	0.049	0.08597	0.0018	core	321.4	97.7	493.9	30.8	531.6	10.4
LM2-16	23850	2372	1052	0.1	0.0747	0.032	0.08043	0.034	0.0078	0.0003	rim	3568.9	58.4	416.4	19.8	50.1	2.2
LM2-17	23971	6302	1218.1	0.26	0.0728	0.043	0.06564	0.038	0.00654	0.0003	rim	4043.9	45.2	572.2	24.7	50.5	1.7
LM2-18	5001	250	157.7	0.05	0.048	0.003	0.05233	0.003	0.0079	0.0002	rim	101	72.1	51.8	2.9	50.7	1
LM2-19	616	29	21.7	0.05	0.0461	0.005	0.05804	0.005	0.00914	0.0005	mixture	901.3	186.2	87.1	12.8	58.7	3.4
LM2-20	146	56	12.8	0.38	0.0575	0.005	0.17282	0.017	0.02178	0.0005	core	512.4	116.6	161.9	15	138.9	3.1
LM2-21	576	176	192.9	0.31	0.0585	0.003	0.6814	0.033	0.0845	0.0014	core	547.1	58	527.6	19.7	523.2	8.5
LM2-22	266	138	381	0.52	0.1245	0.007	5.7038	0.3	0.3327	0.0086	core	2021.1	52.5	1931.9	45.5	1851.6	41.6
LM2-23	78	61	25.6	0.78	0.0565	0.003	0.6191	0.036	0.0794	0.0015	core	473.4	70.5	489.3	22.6	492.8	9.1
LM2-24	132	65	47.7	0.49	0.0584	0.004	0.7423	0.047	0.0921	0.0016	core	546.5	74.9	563.7	27.6	568	9.7
LM2-25	622	302	443	0.49	0.0735	0.004	1.6992	0.076	0.168	0.0049	core	1027	58.9	1008.2	28.5	1000.9	26.9
LM2-26	4915	207	142.9	0.04	0.0489	0.004	0.0523	0.004	0.0078	0.0003	rim	143.7	91.5	51.8	3.6	49.9	1.8
LM2-27	72	43	26.8	0.6	0.0613	0.005	0.7988	0.059	0.0945	0.0019	core	649.2	89.6	596.2	33.3	582.3	11.1
LM2-28	327	181	324.7	0.56	0.0927	0.004	3.2258	0.15	0.2524	0.0045	core	1481.7	49.8	1463.4	36	1450.9	23.4
LM2-29	123	104	139.7	0.85	0.1012	0.005	4.1291	0.188	0.296	0.0052	core	1646	48.1	1660.1	37.1	1671.3	26.1
LM2-30	572	158	324.1	0.28	0.0681	0.003	1.3532	0.065	0.1442	0.0023	core	871.1	55.4	868.9	27.9	868.1	12.7
LM2-31	531	910	89.8	1.71	0.0502	0.003	0.3036	0.016	0.0439	0.0007	core	204.2	67.4	269.2	12.3	276.8	4.5
LM2-32	4868	109	143.4	0.02	0.0486	0.004	0.0532	0.004	0.0079	0.0002	rim	128.9	97.8	52.6	3.6	51	1.5
LM2-33	303	327	125.3	1.08	0.0625	0.003	0.9035	0.045	0.1049	0.0017	core	690.1	59.1	653.6	24	643.1	10.1
LM2-34	182	88	66.9	0.49	0.0606	0.003	0.7834	0.043	0.0938	0.0016	core	624.3	67.2	587.4	24.5	577.9	9.5
LM2-35	501	49	42.1	0.1	0.0508	0.003	0.149	0.01	0.0213	0.0004	core	231.3	84.2	141	8.7	135.7	2.8
LM2-36	376	275	134.8	0.73	0.0641	0.004	0.7962	0.051	0.0902	0.0017	core	743.4	75.6	594.7	28.9	556.5	10.1
LM2-37	9113	110	309.8	0.01	0.0515	0.004	0.0649	0.006	0.0092	0.0004	mixture	261.1	94.5	63.8	5.5	58.7	2.7
LM2-38	149	88	113.1	0.59	0.0772	0.004	2.0866	0.114	0.1961	0.0037	core	1125.8	63.7	1144.4	37.5	1154.4	20.2
LM2-39	1516	510	399.3	0.34	0.0541	0.003	0.4692	0.025	0.063	0.0016	core	373.8	63.3	390.7	17.1	393.6	9.5
LM2-40	402	625	56.3	1.56	0.053	0.003	0.2612	0.017	0.0357	0.0007	core	330.2	79.4	235.6	13.4	226.3	4.4
LM2-41	4858	66	133.1	0.01	0.0498	0.005	0.0507	0.006	0.0074	0.0003	rim	186.4	120.1	50.2	5.4	47.4	2.1
LM2-42	4992	164	144.2	0.03	0.0496	0.006	0.0537	0.007	0.0078	0.0004	rim	177.6	150.1	53.1	6.7	50.4	2.7
LM2-43	2785	80	79.2	0.03	0.0478	0.003	0.0493	0.003	0.0075	0.0002	rim	87.5	85.5	48.9	3.1	48.1	1
LM2-44	7082	313	201.6	0.04	0.0523	0.003	0.0545	0.003	0.0076	0.0002	rim	296.7	76.9	53.9	2.9	48.6	1.1
LM2-45	3989	120	110.2	0.03	0.0502	0.005	0.0515	0.005	0.0074	0.0003	rim	205.9	124.6	51	4.8	47.8	1.8
LM2-46	153	84	13.5	0.55	0.0432	0.005	0.1286	0.013	0.0216	0.0005	core	–114.5	115.1	122.8	11.3	137.8	3.2
LM2-47	7343	577	221.6	0.08	0.0515	0.003	0.0561	0.003	0.0079	0.0002	rim	262	65.7	55.4	3	50.7	1.1
LM248	2327	399	116.4	0.17	0.056	0.004	0.092	0.006	0.0119	0.0003	mixture	452.5	80.6	89.4	5.5	76.4	2

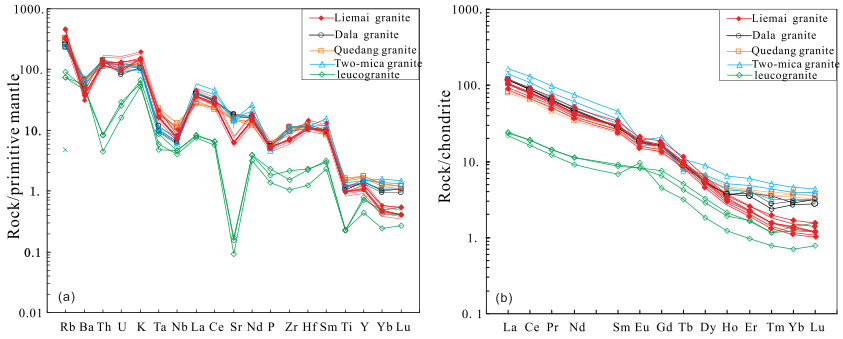

Figure 4. (Colour online) (a) Primitive mantle-normalized trace elements and (b) chondrite-normalized REE distribution patterns for granites and metamorphic rocks from the Yardoi area. Primitive mantle and chondritic normalization values from Pearce, Harris & Tyndall (1984) and Sun & McDonough (1989), respectively.

they are distinct from leucogranites exposed in the core of the Yardoi Dome. The Liemai muscovite-granites are enriched in LILEs (e.g. Rb, K and Ba) and radioactive elements (e.g. U and Th) but are depleted in Ti, Y, Yb and Lu. Elements such as Rb, Th, K, La, Nd, Hf and Y have an obvious positive anomaly, whereas Ba, Nb, Sr, P and Ti have an obvious negative anomaly. In contrast to the two-mica granite from the margin of the Yardoi Dome, the Liemai muscovite-granites have a relatively high Rb content (204.1×10^{-6}–293.8×10^{-6}) and Rb/Sr ratios (1.52–2.20) but a relatively low Sr content ($<134.6\times10^{-6}$) and Sr/Y ratios (23.94–27.73), thus reflecting high amounts of mica minerals.

The Liemai muscovite-granites have lower total rare Earth elements (REEs) ranging over 108.08–113.47 ppm. The REE patterns decline to the right with higher $(La/Yb)_n$ ratios (59.96–79.85) and slightly negative Eu anomalies ($\delta Eu = 0.63$–0.82; Fig. 4b).

The ratios vary from 16.57 to 17.91 for light and heavy REEs (LREE and HREE). The $(La/Gd)_N$ ratios range from 6.28 to 6.51, reflecting the obvious fractionation between LREE and HREE. The LREE patterns are strongly concentrated with respect to the HREE. The Liemai muscovite-granites are distinct from the Miocene leucogranites at Dala and Quedang granites and two-mica granites from the Yardoi Dome. The Liemai granites have medium Sr/Y (23.9–27.7) and La/Sm ratios (5.5–5.6) and high Sm/Yb ratios (15.1–20), indicating a magmatic source with residual phases of amphibole and/or garnet.

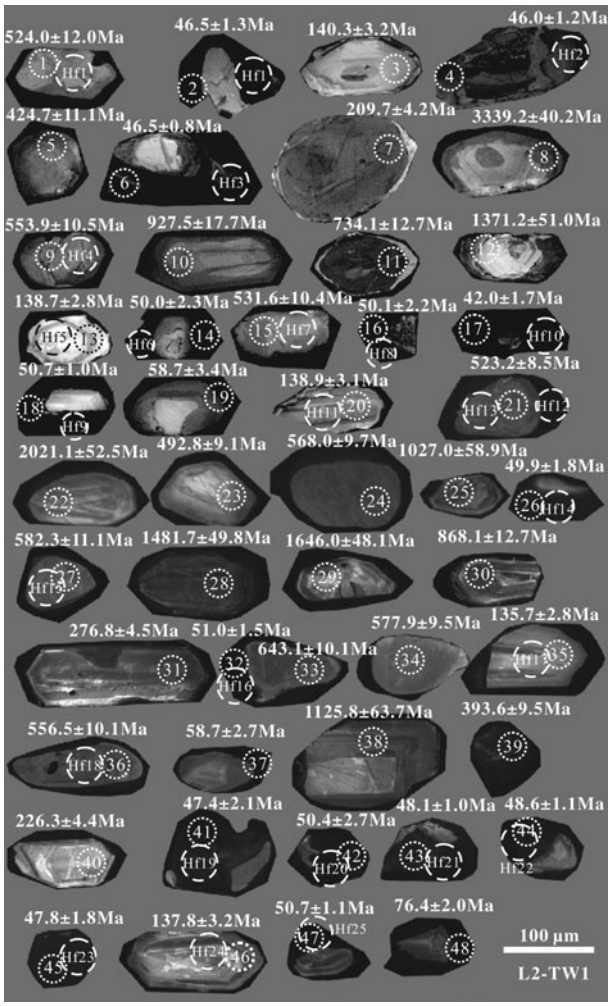

Figure 5. Cathodoluminescence (CL) images and LA-ICP-MS U–Pb ages of zircons from Liemai muscovite-granites (large white circles denote the spot Hf analysis, while the smaller dash-dot circles represent U–Pb dating spot).

4.b. Zircon geochronology

U–Pb ages were determined on zircons separated from the Liemai muscovite-granite samples. The results are listed in online Supplementary Table S2. Zircons are commonly 50–200 μm in length and have prismatic euhedral-subhedral shapes (Fig. 5), with length-to-width ratios of 1:1 to 2:1, up to 3:1 in some individual zircons. The zircon crystals commonly have a core–rim structure, and some grains have a dark and complex internal texture and overgrown rims (Fig. 5) under the CL imager. Zircon rims have varying widths and weak CL without oscillatory zoning structures. The darker colour of the zircon rims has a strong association with high U and Th concentrations and resultant metamictization (Wu *et al.* 2015), suggestive of a magmatic origin by anatectic partial melting (Wu & Zheng, 2004). The inherited zircon cores are light in colour, sub-rounded or irregular in shape, and have a strong CL and internal embayed

https://doi.org/10.1017/S0016756817000966 Published online by Cambridge University Press

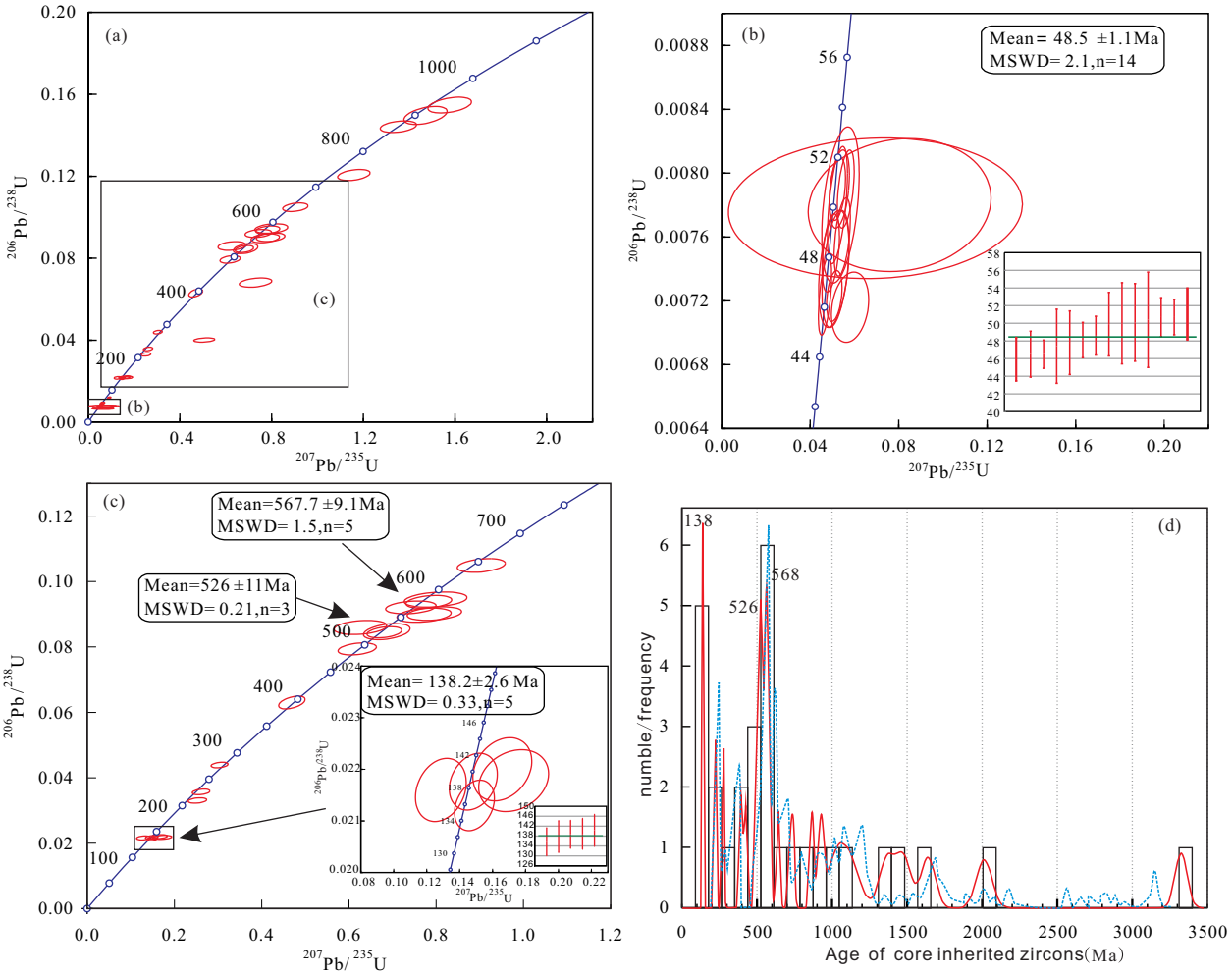

Figure 6. (Colour online) U–Pb Concordia diagrams for zircons from Liemai muscovite-granites: (a) zircon U–Pb concordia diagrams; (b) concordia diagram for zircon rims; (c) concordia diagram for inherited zircon cores; and (d) distribution curves of inherited zircon cores and detrital zircons.

dissolution phenomenon. A few inherited zircon cores have magmatic oscillatory zoning. Zircon crystals with relatively wider cores and rims were selected for U–Pb dating by LA-ICP-MS. The analytical results are listed in Table 2.

Eighteen analyses were performed on the rim, but the results of several analytical spots (nos 19, 37 and 48) were excluded from calculations due to probable mixing with inherited zircon cores. The other 15 effective analyses show high U and Th concentrations in the zircon rims, ranging from 2785×10^{-6} to 23850×10^{-6} and 26×10^{-6} to 2372×10^{-6}. The low Th/U ratios of the zircon rims (< 0.1) combined with internal textural characteristics are consistent with an anatectic melting origin for the leucogranite. Some spots (nos L2-14, -16 and -17) are characterized by high U concentrations. In CL images the rims are commonly black due to their high U content; however, the nearly constant $^{206}Pb/^{238}U$ ages with large variations in U contents (10181–23971 ppm) indicates that the U–Pb system was not substantially affected by the high U concentrations. In addition, these spots are also characterized by low Th/U ratios; the well-developed oscillatory zoning indicates that they grew from granitic melts.

Among 15 analyses of spots with oscillatory zoning, 14 spots have a relatively high concordance (≥95 %) and a relative narrow range of $^{206}Pb/^{238}U$ ages, varying from 47.4 ± 2.1 Ma to 51.0 ± 1.5 Ma (Fig. 6b; Table 2), with a weighted average age of 48.5 ± 1.1 Ma (n = 14; MSWD=2.1). This group of ages is relatively concentrated on the concordia diagrams (Fig. 6) and is considered highly reliable. These ages are interpreted as crystallization ages for the Liemai muscovite-granites.

According to the results of 30 analyses, inherited zircon cores have relatively lower U and Th concentrations, varying from 70×10^{-6} to 622×10^{-6} and from 43×10^{-6} to 910×10^{-6}, respectively, with Th/U ratios greater than 0.1 (0.1–1.71). $^{206}Pb/^{238}U$ data are used for inherited zircons having ages lower than 1000 Ma, whereas $^{207}Pb/^{206}Pb$ data are used for inherited zircons having ages greater than 1000 Ma. The age span is considerable in the inherited zircon cores, ranging from 135.7 ± 35.7 Ma to 3339.2 ± 40.2 Ma (Fig. 6d; Table 2).

https://doi.org/10.1017/S0016756817000966 Published online by Cambridge University Press

Table 3. Hf isotopic composition of zircons from Liemai granite

Sample	$^{176}Yb/^{177}Hf$	2σ	$^{176}Lu/^{177}Hf$	2σ	$^{176}Hf/^{177}Hf$	2σ	Age (Ma)	$\varepsilon_{Hf}(0)$	$\varepsilon_{Hf}(t)$	2σ	T_{DM1} (Ma)	±2σ	T_{DM2} (Ma)	±2σ
Hf1	0.006467	0.000106	0.00022	0.000004	0.282215	0.000012	526	−19.7	−8.2	0.7	1433	33	1818	53
Hf2	0.030748	0.000592	0.001002	0.000019	0.282621	0.000011	138	−5.3	−2.4	0.6	893	31	1191	49
Hf3	0.036918	0.000507	0.001044	0.00002	0.282644	0.000021	48.5	−4.5	−3.5	0.9	862	59	1182	94
Hf4	0.023826	0.00019	0.000732	0.000004	0.282576	0.000011	48.5	−6.9	−5.9	0.7	950	31	1316	49
Hf5	0.025718	0.000354	0.000858	0.000009	0.282387	0.000011	568	−13.6	−1.7	0.7	1217	31	1483	49
Hf6	0.026659	0.000398	0.000874	0.000015	0.282652	0.000013	138	−4.3	−1.3	0.7	847	37	1130	58
Hf7	0.013842	0.000774	0.000436	0.000029	0.282565	0.000008	48.5	−7.3	−6.2	0.6	958	22	1335	36
Hf8	0.010763	0.000123	0.000354	0.000003	0.282206	0.000012	526	−20	−8.5	0.7	1450	33	1835	53
Hf9	0.033277	0.00135	0.001022	0.000039	0.282676	0.000013	48.5	−3.4	−2.3	0.7	816	37	1118	58
Hf10	0.032214	0.000146	0.000891	0.000008	0.28261	0.000011	48.5	−5.7	−4.7	0.6	906	31	1247	49
Hf11	0.034938	0.002257	0.000962	0.000053	0.282597	0.000013	48.5	−6.2	−5.1	0.7	926	37	1273	58
Hf12	0.032291	0.001735	0.001017	0.000055	0.282698	0.000011	138	−2.6	0.3	0.7	785	31	1040	49
Hf13	0.002889	0.000149	0.000096	0.000006	0.282214	0.000009	526	−19.7	−8.3	0.6	1430	25	1818	40
Hf14	0.008101	0.000086	0.000281	0.000002	0.282082	0.000013	568	−24.4	−12	0.7	1617	35	2059	58
Hf15	0.03869	0.001114	0.001324	0.000022	0.282582	0.000014	48.5	−6.7	−5.7	0.7	957	40	1304	63
Hf16	0.043088	0.001255	0.001415	0.000042	0.282561	0.000023	48.5	−7.5	−6.4	1	989	65	1346	103
Hf17	0.032964	0.001376	0.001088	0.00005	0.282718	0.000012	138	−1.9	1	0.7	759	34	1003	54
Hf18	0.017339	0.000392	0.000552	0.000012	0.28242	0.000015	568	−12.4	−0.4	0.8	1162	42	1411	67
Hf19	0.021929	0.00048	0.000732	0.000012	0.28258	0.000011	48.5	−6.8	−5.7	0.6	944	31	1306	49
Hf20	0.034637	0.000879	0.001092	0.000028	0.282631	0.000011	48.5	−5	−3.9	0.6	882	31	1207	49
Hf21	0.031166	0.00131	0.000988	0.000046	0.282577	0.000012	48.5	−6.9	−5.8	0.7	955	34	1313	54
Hf22	0.022551	0.000764	0.000715	0.000025	0.282597	0.000009	48.5	−6.2	−5.2	0.6	920	25	1274	40
Hf23	0.042729	0.002858	0.001346	0.00008	0.282621	0.000027	48.5	−5.3	−4.3	1.1	902	77	1227	121
Hf24	0.043415	0.002464	0.001346	0.000076	0.282741	0.000018	138	−1.1	1.8	0.8	731	51	957	81
Hf25	0.011833	0.001484	0.000365	0.000049	0.28265	0.000021	48.5	−4.3	−3.2	0.9	839	58	1169	94

$\varepsilon_{Hf}(t) = 10\,000\times\{[(^{176}Hf/^{177}Hf)_S - (^{176}Lu/^{177}Hf)_S \times (e^{\lambda t} - 1)]/[(^{176}Hf/^{177}Hf)_{CHUR,0} - (^{176}Lu/^{177}Hf)_{CHUR} \times (e^{\lambda t} - 1)] - 1\}$, $T_{DM1} = (1/\lambda) \times \ln\{1 + [(^{176}Hf/^{177}Hf)_S - (^{176}Hf/^{177}Hf)_{DM}] / [(^{176}Lu/^{177}Hf)_S - (^{176}Lu/^{177}Hf)_{DM}]\}$, $T_{DM2} = T_{DM1} - (T_{DM1} - t) \times [(f_{cc} - f_s)/(f_{cc} - f_{DM})]$ and $f_{Lu/Hf} = (^{176}Lu/^{177}Hf)_S/(^{176}Lu/^{177}Hf)_{CHUR} - 1$, where $\lambda = 1.867\times10^{-11}$ (a^{-1}) (Söderlund *et al.* 2004); $(^{176}Lu/^{177}Hf)_S$ and $(^{176}Hf/^{177}Hf)_S$ are the measured values of the samples; $(^{176}Lu/^{177}Hf)_{CHUR} = 0.0332$, $(^{176}Hf/^{177}Hf)_{CHUR,0} = 0.282772$, $(^{176}Lu/^{177}Hf)_{DM} = 0.0384$ and $(^{176}Hf/^{177}Hf)_{DM} = 0.28325$ (Griffin *et al.* 2000); $(^{176}Lu/^{177}Hf)_{mean\ crust} = 0.015$; $f_{cc} = [(^{176}Lu/^{177}Hf)_{mean\ crust}/(^{176}Lu/^{177}Hf)_{CHUR}] - 1$; $f_s = f_{Lu/Hf}$; and $f_{DM} = [(^{176}Lu/^{177}Hf)_{DM}/(^{176}Lu/^{177}Hf)_{CHUR}] - 1$.

The inherited zircon cores have three age peaks: 138, 526 and 568 Ma. Analytical spot nos 3, 13, 20, 35 and 48 of the inherited zircon cores have clear oscillatory zoning, with U and Th concentrations varying from 146×10^{-6} to 501×10^{-6} and 49×10^{-6} to 84×10^{-6}, respectively. The Th/U ratios are greater than 0.1 (0.10–0.55), and the $^{206}Pb/^{238}U$ ages are concentrated within a range of 135.7–140.3 Ma. Zircon inherited cores are clustered around *c.* 138 Ma on the $^{206}Pb/^{238}U$ concordia diagram, with a weighted mean age of 138.2 ± 2.6 Ma (MSWD=0.33) (Fig. 6c). This group of ages is relatively concentrated on the concordia diagram, reflecting high reliability and indicating that the source of the Liemai muscovite-granite contained Late Jurassic – Early Cretaceous zircons.

The other peak age of the inherited zircon cores are 523 Ma and 582 Ma. The oscillatory zoning of the inherited zircon cores of these ages is implicit. These inherited zircon cores have U and Th concentrations of 70×10^{-6} to 576×10^{-6} and 43×10^{-6} to 343×10^{-6}, respectively, with Th/U ratios varying from 0.31 to 1.63. The resultant $^{206}Pb/^{238}U$ may be divided into two groups. The $^{206}Pb/^{238}U$ ages of analytical spot nos 1, 15 and 21 are between 523.2 and 531.6 Ma, with a weighted mean age of 526 Ma ($n = 3$; MSWD=0.21). The $^{206}Pb/^{238}U$ ages of analytical spots 9, 24, 27, 34 and 36 range from 553.9 ± 10.1 Ma to 582.3 ± 11.1 Ma and are concentrated around 568 Ma, with a weighted mean age of 567.7 ± 9.1 Ma ($n = 5$; MSWD=1.50) (Fig. 6c). The 523–582 Ma age indicates that the source rocks of the Liemai leucogranite contained early Palaeozoic – Neoproterozoic zircon crystals. The other inherited zircon cores have ages of 643–3339.2 Ma, reflecting multiple sources of inherited zircons. The oldest (age 3339 Ma) is obtained from analytical spot no. 9, which suggests that it was crystallized as early as during Palaeoarchean time. The inherited zircon grains might be derived from its source or captured from the wall rocks during the ascent of the granitic magma.

4.c. Zircon Hf isotope characteristics

Based on the U–Pb dating results, a total of 14 representative analytical spots on rims and 11 on inherited zircon cores were selected and measured for *in situ* Lu–Hf isotopic compositions using LA-MC-ICP-MS. The analytical results are listed in Table 3. All zircon crystals have $^{176}Lu/^{177}Hf$ ratios less than 0.002, reflecting extremely low accumulations of the radioactive Hf isotope after zircon crystallization (Wu *et al.* 2007). Zircon rims dated to 48.5 Ma have relatively homogeneous Hf isotope compositions, with $^{176}Hf/^{177}Hf$ ratios that vary between 0.282561 and 0.282676. Their initial Hf isotope compositions ($\varepsilon_{Hf}(t)$) range from –6.4 to –2.3, with an average of –4.9. The two-stage depleted mantle model ages (T_{DM2}) range from 1118 to 1346 Ma, which indicate that they may be derived from products of Mesoproterozoic crustal reworking. Inherited zircon cores that date to 138 Ma have little

https://doi.org/10.1017/S0016756817000966 Published online by Cambridge University Press

variation in their $^{176}Hf/^{177}Hf$ ratios (0.282621–0.282741). Their initial Hf isotope compositions ($\varepsilon_{Hf}(t)$) vary from –2.4 to 1.8, with an average of –0.6. The two-stage depleted mantle Hf model ages vary from 1430 to 1450 Ma, which indicates that its source rocks were Mesoproterozoic. Inherited zircon cores dated to 526 Ma have indistinguishable $^{176}Hf/^{177}Hf$ ratios (0.282206–0.282215). Their initial Hf isotope compositions ($\varepsilon_{Hf}(t)$) vary from –8.5 to –8.2. Hf model ages vary from 1430 to 1450 Ma, indicating that its source rocks were Mesoproterozoic crustal rocks.

5. Discussion

5.a. Chronology of the granite

Tethyan Himalayan leucogranites (THL) are predominantly muscovite-biotite leucogranites and muscovite-tourmaline leucogranites. Previous studies have shown that these leucogranites have variable crystallization ages ranging over 8–45 Ma for the THL. Leucogranites with ages of 26–46 Ma are mainly distributed in the Tethyan Himalaya (Wu *et al.* 2015). Magmatic activities around the Yardoi Dome were constrained to 45–15 Ma and may be divided into three periods: (1) 45–40 Ma: includes the Dala, Quedangyan, two-mica granitic dykes and rhyolitic subvolcanic rocks intruded into the central Yardoi Dome (Aikman, Harrison & Lin, 2008; Qi *et al.* 2008; Hu *et al.* 2011; Zeng *et al.* 2011; Wu *et al.* 2014); (2) *c.* 35 Ma: formation of granitic dykes within the Yardoi Dome (Gao *et al.* 2009; Zeng *et al.* 2009; Wu *et al.* 2014); and (3) *c.* 15 Ma: formation of leucogranite within the core of the Yardoi Dome (Wu *et al.* 2014). Zircon rims from the Liemai muscovite-granites, which intruded in the eastern dome, show 'black zircon' characteristics that are consistent with those of zircons from the Himalayan leucogranites. The LA-ICP-MS analytical results showed that zircon rims have a relatively limited range of ages of 47.4–51.0 Ma, with a weighted mean age of 48.5 ± 1.1 Ma (MSWD=1.6), reflecting the crystallization and intrusion ages of the Liemai muscovite-granites. These ages are consistent with the metamorphic age (47.6 Ma) of the biotite-bearing granitic genesis from the Yardoi Dome (Gao, Zeng & Xie, 2012). This age has changed the intrusion age of the Himalayan leucogranite by 3 Ma, indicating the existence of magmatic activity in the Himalayan region as early as 48.5 Ma.

5.b. Source region of granite

It is generally accepted that the High Himalayan leucogranites were derived from metamorphic mudstones of the High Himalayan Crystallization System (HHCS) (Harris & Inger, 1992; Harrison *et al.* 1999; Guo & Li, 2007; Huang *et al.* 2013), whereas the source of the Tethyan Himalaya leucogranite (THL) remains controversial. The source may be similar to the Miocene

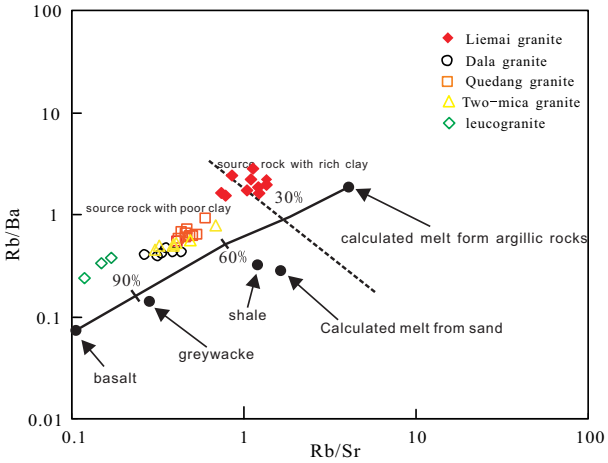

Figure 7. (Colour online) Plot of Rb/Ba v. Rb/Sr for Liemai muscovite-granites (after Sylvester, 1998).

leucogranites (Zhang *et al.* 2004, 2005; Liao *et al.* 2007; Yu *et al.* 2011; Gao *et al.* 2013).

The Eocene two-mica granites of Yardoi gneiss dome possibly represent the partial melting products from amphibolite with minor contributions from metapelite under contraction and thickening conditions (Gao *et al.* 2009; Zeng *et al.* 2009, 2011). The aluminium saturation index of the Liemai muscovite-granites (A/CNK) is greater than 1.1. The CIPW calculation has over 2 % corundum (2.68–3.06 %). These features indicate that the Liemai muscovite-granites belong to muscovite-bearing K-rich strong peraluminous S-type granites that originate from the crust. The CaO/Na_2O ratio may be used as a source composition tracer (Sylvester, 1998). Partial melting of pelite that is enriched in clay but depleted in plagioclase may generate melt with relatively low CaO/Na_2O ratios (<0.3). Melts of sandstone enriched in plagioclase but depleted in clay minerals generally have relatively higher CaO/Na_2O ratios (>0.3). The aluminous felsic melt derived from partial melting of pelite under conditions of water saturation usually has a high Sr/Ba ratio (0.5–1.6) and low CaO/Na_2O ratio. The Liemai granites have CaO/Na_2O ratios ranging from 0.22 to 0.28 and Sr/Ba ratios from 0.5 to 0.6, indicating that the source of granite is a plagioclase-depleted but clay-mineral-enriched pelite region. On a Rb/Ba – Rb/Sr diagram (Fig. 7), granites from near the Yardoi Dome have an apparent linear correlation. Compared to the Dala and QueDang granites, the Liemai muscovite-granites tend to plot in a clay-mineral-rich source region. The rim with oscillatory zoning of zircons from Leimai granite has $\varepsilon_{Hf}(t)$ ranging from –6.4 to –2.3, with an average of –4.9. These observations indicate an origin from recycled old crust, which is distinct from the high Himalayan leuocogranite (Huang *et al.* 2013).

S-type granites commonly have inherited zircon crystals. *In situ* U–Pb dating and Lu–Hf isotope analyses of the inherited zircons are important for identifying the granite source materials and constraining the nature and source of crustal materials (Zhao, Zheng

https://doi.org/10.1017/S0016756817000966 Published online by Cambridge University Press

& Dai, 2013). The Liemai muscovite-granite contains a large amount of inherited zircon. LA-ICP-MS U–Pb dating of the inherited zircons shows a remarkable range spanning 135.7–3339.2 Ma, reflecting multiple sources of inherited zircon. Inherited zircon cores have a prominent peak age of 135–140 Ma, with a weighted mean age of 138.2 Ma. These inherited zircon cores have bright colours on CL imagery and are characterized by apparent oscillatory zoning and high Th/U ratios, indicating a magmatic origin. The Longzi-Qiaga rhyolitic subvolcanic rocks and Dala and Quedang two-mica granites from the southern Yardoi Dome contain inherited zircon with ages that vary over the range 126–144 Ma (Hu *et al.* 2011; Zeng *et al.* 2011; Wu *et al.* 2014). Biotite-bearing granitic gneiss from the Yardoi Dome also contains inherited zircons with ages of 135.2 ± 1.6 Ma and 136.1 ± 1.4 Ma (Gao, Zeng & Xie, 2012). In addition, inherited zircons with ages of 131–142 Ma are found in two-mica granites and granitic gneiss from the Ranba Dome in the western Tethyan Himalaya (Liu *et al.* 2014). These data indicate that inherited zircon crystals were common parts of granites and metamorphic rocks surrounding the Yardoi Dome during Late Jurassic – Early Cretaceous time and may be pervasive in the Eocene Tethyan Himalaya leucogranites and high-grade metamorphic rocks from the central Yardoi Dome. No similar ages have been recorded in zircons from the High Himalayan sedimentary rock series, excluding it as a possible source for the Tethyan Himalaya leucogranite.

Zircon Hf isotope has widely been used in source discrimination of some important geochemical reservoirs (such as depleted mantle, chondrite and crustal) (Griffin *et al.* 2000; Wu *et al.* 2007). Low $^{176}Hf/^{177}Hf$ ratios and $\varepsilon_{Hf}(t)$ values in zircons are considered to be derived from or contaminated by crust, whereas rocks with higher $^{176}Hf/^{177}Hf$ ratios and $\varepsilon_{Hf}(t)$ values demonstrate significant input of depleted mantle material or juvenile crust, which means that the mantle material played a vital role in the formation of the granites (Kinny & Maas, 2003).

The newly produced zircon rim yields negative zircon $\varepsilon_{Hf}(t)$ values spread over a range of –6.4 to –2.3, and T_{DM2} of 1118–1346 Ma. All the data points fall within the lower crust region. Hf isotope composition of inherited zircon cores have variable $\varepsilon_{Hf}(t)$ from –12 to –0.4, and all the data points except three (0.3, 1, 1.8) lie near the chondrite evolution line, above the evolution curve of the lower crust and below the evolution curve of chondrite. These data indicate that the Liemai muscovite-granite is derived mainly from anatexis/reworking of the ancient crust. The wide range of $\varepsilon_{Hf}(t)$ values might reflect inherited zircon components or mixing of old and juvenile crustal material. The other age peaks of inherited zircon cores vary from 523 to 582 Ma and have two populations: 526 ± 11 Ma and 567.7 ± 9.1 Ma. Slightly younger zircon ages have been reported in granitic gneiss of the Yardoi Dome (Gao, Zeng & Xie, 2012) and in eyeball-shaped mylonites of the southeastern Yardoi Dome (520.4 ± 6.3 Ma) and Dala granites (536 ± 12.3 Ma) (Wu *et al.* 2014). The frequency distribution patterns of inherited zircon crystals from the Liemai muscovite-granites are consistent with those of leucogranites from the Ramba Dome (Liu *et al.* 2014). Furthermore, the age spectrum of this sample is close to that of the surrounding Tethyan sedimentary strata (Aikman, Harrison & Lin, 2008; Liu *et al.* 2014). Generally speaking, incomplete melting of source rocks or assimilation of country rocks are the two possibilities for the origin of the inherited zircon. However, remnants of the source usually do not survive during the long process of fractionation. The close affinity between the inherited zircons and the surrounding country rocks also suggests that the inheritable zircons were probably captured from country-rock xenoliths during magma ascent towards the surface. In addition, the zircon grains usually show sharp and regular boundaries between the inherited cores and the overgrowths, indicating limited dissolution of the inherited zircons.

Based on the above analyses, inherited zircon crystals from the Liemai muscovite-granite are not from metapelite of the High Himalayan Crystallization Series. The presence of zircons inherited from the country rocks indicates a certain degree of crustal assimilation during magma evolution.

The Liemai muscovite-granites are similar to the previously reported North Himalayan granites in that they contain high concentrations of SiO_2, low concentrations of MgO, CaO, and Fe_2O_3, have low CaO/Na_2O and Al_2O_3/TiO_2 ratios, and have negative $\varepsilon_{Hf}(t)$ values, indicating that they formed from magmas derived from a metasedimentary-dominated source region. The Eocene Tethys–Himalaya leucogranite and gneiss of the Yardoi Dome have similar detrital zircon records. Under the condition of crust thickening induced by the India–Eurasia collision, granitic gneiss and mylonite were assimilated in the deep crust and partially melted, forming the Tethyan Himalaya Eocene leucogranite.

5.c. Tectonic environment and petrogenesis

The dehydrated partial melting of muscovite is an important mechanism for the formation of the Tethyan Himalaya Miocene leucogranite (Zhang *et al.* 2004, 2005; Qi *et al.* 2008; Yu *et al.* 2011; Zeng *et al.* 2012; Gao & Zeng, 2014). The Dala and Quedang two-mica granites within and surrounding the Yardoi Dome were formed under conditions of crustal thickening, mainly by the dehydrated partial melting of amphibolite within crustal mafic lithologies, in combination with subsidiary partial melting of metapelite (Gao *et al.* 2009; Zeng *et al.* 2009, 2011; Xie *et al.* 2010). Although strongly peraluminous granite located at different temporal-spatial conditions within the Tibetan Plateau may not be identical in terms of its genetic mechanism and tectonic significance, all granites were products of middle–upper crust anatectic melting under conditions of relatively low temperature and high

https://doi.org/10.1017/S0016756817000966 Published online by Cambridge University Press

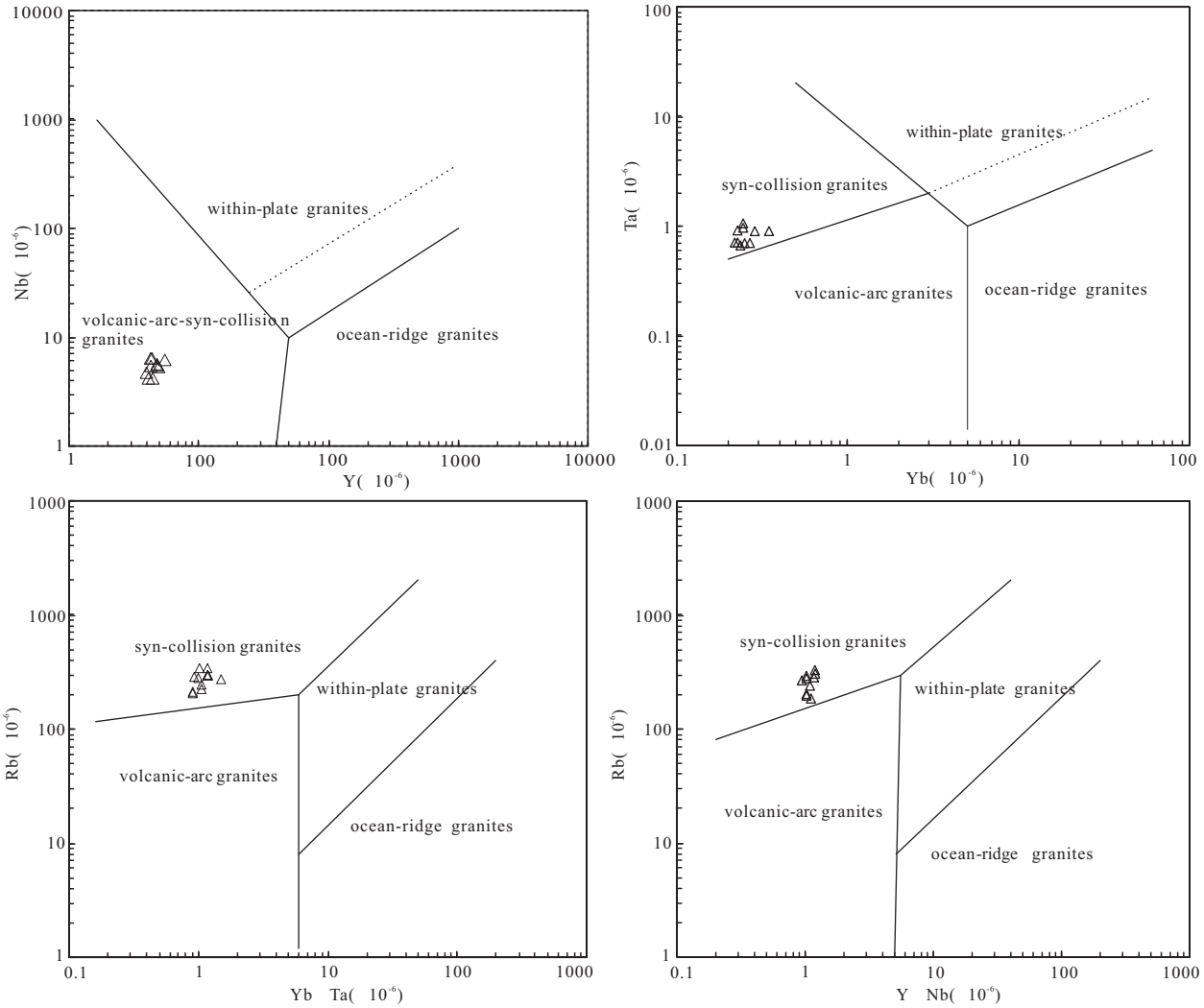

Figure 8. Trace-element discriminant diagrams for tectonic settings (after Pearce, Harris & Tindle, 1984).

pressure during the collision – post-collision phase (Mo, 2009).

Zircon U–Pb dating results have shown that metamorphism of garnet amphibolite and gneiss from the Yardoi Dome occurred during 47.6–45.0 Ma (Gao, Zeng & Xie, 2012).

The Liemai muscovite-granite has a crystallization age that is consistent with the metamorphism of the gneiss but is apparently earlier than garnet amphibolite metamorphism. It indicates that earlier partial melting, as represented by the Liemai granite, was mainly metapelite partial melting, accompanied by a lower degree of melting of mafic lithologies. This difference is also reflected in the geochemistry of the Liemai muscovite-granite and in the Dala and Quedang two-mica granite. The features of the Liemai muscovite-granite, such as the high Rb concentration, low Sr concentration, high Rb/Sr ratio (Rb/Sr > 1.0), and low Ca and Sr concentration, show an elevated amount of negative Eu anomalies, a characteristic effect induced by fractional crystallization of plagioclase. Magmatic differentiation preceded by plagioclase fractional crystallization therefore probably played a critical role in the production of peraluminous leucogranitic melts, which is generally considered a product of the dehydrated partial melting of muscovite from metapelite. During the early stages of partial melting, clay-rich pelite is more vulnerable to partial melting because Rb has an affinity to mica minerals and Sr tends to concentrate in feldspar minerals. This would lead to the dehydrated partial melting of muscovite, which would increase the Rb/Sr ratio of the melt (Zeng, Asimow & Saleeby, 2005). Garnet remains in the residues lead to the depletion of HREE in melt, whereas concentrations in residual gneiss and amphibolites may lead to melts highly enriched in HREE, gneiss and amphibolites. As the partial melting of mafic lithology increases, the plagioclase melts and forms two-mica granite.

Previous studies have shown that the initial India–Eurasia collision occurred at *c.* 65 Ma and continued until 41 Ma (Ding *et al.* 2003; Mo, 2003; Hou *et al.* 2006). Ji *et al.* (2016) proposed that the extensive early Cenozoic tectonomagmatic evolution of southern Tibet can be described by the Neo-Tethyan slab break-off model. Based on the ages of the gabbros which come from partial melting of the asthenosphere followed by rapid magma ascent with negligible crustal contamination, Ji *et al.* (2016) inferred that break-off

https://doi.org/10.1017/S0016756817000966 Published online by Cambridge University Press

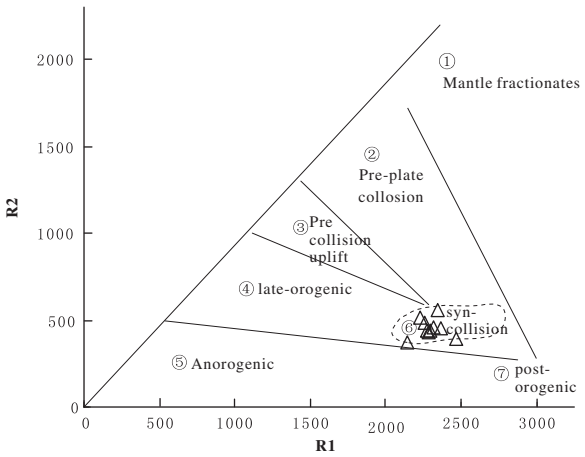

Figure 9. Discriminant diagrams of tectonic setting for R1 v. R2.

occurred at *c.* 45 Ma. The break-off model may account for coeval tectonomagmatic activities in southern Tibet. The Liemai muscovite-granite intruded into the Tethyan Himalaya terrane, which is the footwall of the subduction zone. Zircon U–Pb dating reveals an intrusion age of the granite of 48.5 Ma, in accordance with the main collision stage. In addition, on the trace-element tectonic environment discrimination diagram (Fig. 8) and R_1–R_2 multiple cation parameters tectonic discrimination diagram (Fig. 9), all samples plot in the syn-collision granite area, further confirming that the Liemai muscovite-granites were formed during continental collision.

The Himalayan orogenic belt experienced earlier dominantly contraction and thickening and later contemporaneous contraction and extension. Such a change in the tectonic regime was accompanied by a transition in the partial melting of the deep crustal rocks (Zeng *et al.* 2015).

Intense crustal shortening during the main collision stage led to temperature and pressure increases in the deep crust, which induced the generation of peraluminous granites which experienced intensive partial melting under contraction and thickening conditions. Combined with zircon U–Pb dating and the tectonic environment, the Liemai muscovite-granite is genetically related to the main stage of the India–Eurasia collision when crustal thickening induced partial melting, and is a response of the footwall of the subduction zone to continental collision. We demonstrate that Liemai muscovite-granite in the Eastern Tethyan Himalayan underwent early Eocene intense anatexis under contraction and thickening conditions due to shallow subduction of the Indian continent beneath southeastern Tibet.

6. Conclusions

The U–Pb ages of zircon rims from the Liemai muscovite-granite are 48.5 ± 1.1 Ma and are crystallization ages. This age is *c.* 2 Ma older than the previously published ages of the Tethyan Himalaya leucogranite. The initial Hf isotope $\varepsilon_{Hf}(t)$ is between –6.4 and –2.3, indicating a crustal origin. The rocks are peraluminous high-K calc-alkaline granites, with REE distribution patterns and trace-element concentrations comparable to those of Eocene leucogranites from the Yardoi Dome.

Inherited zircon cores from the Liemai muscovite-granite have a wide range of U–Pb ages that span 135.7–3339.2 Ma, which is interpreted as a result of various source regions.

The Liemai muscovite-granites were formed in a collisional environment. These magmas were derived mainly from the anatexis of ancient crustal materials under contraction and thickening conditions due to subduction of the Indian continent beneath southeastern Tibet. Crustal thickening and increasing pressure and temperature induced partial melting of middle–lower crustal material. Anatectic magmatism has been attributed to break-off of the Neo-Tethyan slab.

Acknowledgements. We thank Dr Jiang Junsheng for help with the LA-ICP-MS analysis, and special thanks are extended to Dr Tian Kan for help with Hf analysis. The research was financially supported by the National Natural Science foundation of China (grant no. 41402098), the Geological Survey Project of Chinese (grant nos 1212011220664 and 1212011121250) and the Research Foundation of Chengdu University of Technology (No. 2017YG07).

Supplementary material

To view supplementary material for this article, please visit https://doi.org/10.1017/S0016756817000966

References

Aikman, A. B., Harrison, T. M. & Lin, D. 2008. Evidence for early (>44 Ma) Himalayan crustal thickening, Tethyan Himalaya, southeastern Tibet. *Earth and Planetary Science Letters* **274**, 14–23.

Ding, L., Kapp, P., Zhong, D. & Deng, W. 2003. Cenozoic volcanism in Tibet: evidence for a transition from oceanic to continental subduction. *Journal of Petrology* **44**, 1833–65.

Gao, L. & Zeng, L. 2014. Fluxed melting of metapelite and the formation of Miocene high-CaO two-mica granites in the Malashan gneiss dome, southern Tibet. *Geochimica et Cosmochimica Acta* **130**, 136–55.

Gao, L., Zeng, L., Hou, K., Guo, C., Tang, S., Xie, K. & Wang, L. 2013. Episodic crustal anatexis and the formation of Paiku composite leucogranitic pluton in the Malashan Gneiss Dome, Southern Tibet. *Chinese Science Bulletin* **58**, 3546–63.

Gao, L., Zeng, L. & Hu, G. 2010. High Sr/Y two-mica granite from Quedang area, southern Tibet, China: Formation mechanism and tectonic implications. *Geological Bulletin of China* **29**, 214–26.

Gao, L., Zeng, L., Liu, J. & Xie, K. 2009. Early oligocene Na-rich peraluminous leucogranites in the Yardoi Gneiss Dome, Southern Tibet: formation mechanism and tectonic implications. *Acta Petrologica Sinica* **25**(9), 2289–302.

Gao, L., Zeng, L. & Xie, K. 2012. Eocene high grade metamorphism and crustal anatexis in the North Himalaya

Gneiss Domes, Southern Tibet. *Chinese Science Bulletin* **57**, 639–50.

Griffin, W. L., Pearson, N. J., Belousova, E., Jackson, S. E., Van Achterbergh, E., O'Reilly, S. Y. & Shee, S. R. 2000. The Hf isotope composition of cratonic mantle: LAM-MC-ICPMS analysis of zircon megacrysts in kimberlites. *Geochimica et Cosmochimica Acta* **64**, 133–47.

Guo, S., & Li, S. 2007. Petrological and geochemical constraints on the origin of leucogranites. *Earth Science Frontiers* **14**, 290–8.

Harris, N. B. W. & Inger, S. 1992. Trace element modelling of pelite-derived granites. *Contributions to Mineralogy and Petrology* **110**, 46–56.

Harrison, M. T., Grove, M., Mckeegan, K. D., Coath, C. D., Lovera, O. M. & Fort, P. L. 1999. Origin and episodic emplacement of the Manaslu intrusive complex, central Himalaya. *Journal of Petrology* **40**, 3–19.

Hou, Z., Mo, X., Yang, Z., Wang, A., Pan, G., Qu, X. & Nie, F. 2006. Metallogeneses in the collisional orogen of the Qinghai-Tibet Plateau: Tectonic setting, tempospatial distribution and ore deposit types. *Geology in China* **33**, 347–51.

Hu, G., Zeng, L., Qi, X., Hou, K. & Gao, L. 2011. The Mid-Eocene subvolcanic field in the Lhunze-Qiaga area, Tethyan Himalaya, southern Tibet: a high-level magmatic suite related to the Yardoi two-mica granite. *Acta Petrologica Sinica* **27**, 3308–18.

Hu, Z., Liu, Y., Gao, S., Liu, W., Zhang, W., Tong, X. & Zhou, L. 2012. Improved in situ Hf isotope ratio analysis of zircon using newly designed X skimmer cone and jet sample cone in combination with the addition of nitrogen by laser ablation multiple collector ICP-MS. *Journal of Analytical Atomic Spectrometry* **27**, 1391–9.

Huang, C., Zhao, Z., Zhu, D., Liu, D., Hu, Y., Dong, M. & Zhang, J. 2013. Geochemistry, zircon U-Pb chronology and Hf isotope of Luozha leucogranite, southern Tibet: implication for petrogenesis. *Acta Petrologica Sinica* **29**, 3689–702.

Ji, W., Wu, F., Chung, S., Wang, X., Liu, C., Li, Q. & Wang, J. 2016. Eocene Neo-Tethyan slab breakoff constrained by 45 Ma oceanic island basalt-type magmatism in southern Tibet. *Geology* **44**, 283–6.

Kinny, P. D. & Maas, R. 2003. Lu–Hf and Sm–Nd isotope systems in zircon. *Reviews in Mineralogy and Geochemistry* **53**, 327–41.

Liao, Z., Mo, X., Pan, G., Zhu, D., Wang, L., Jiang, X. & Zhao, Z. 2007. Spatial and temporal distribution of peraluminous granites in Tibet and their tectonic significance. *Journal of Asian Earth Sciences* **29**, 378–89.

Liu, Y., Gao, S., Hu, Z., Gao, C., Zong, K. & Wang, D. 2010. Continental and oceanic crust recycling-induced melt–peridotite interactions in the Trans-North China Orogen: U–Pb dating, Hf isotopes and trace elements in zircons from mantle xenoliths. *Journal of Petrology* **51**, 537–71.

Liu, Z., Wu, F., Ji, W., Wang, J. & Liu, C. 2014. Petrogenesis of the Ramba leucogranite in the Tethyan Himalaya and constraints on the channel flow model. *Lithos* **208**, 118–36.

Mo, X. 2009. A review of genesis study on magmatic rocks of the Qinghai-Tibet Plateau: achievements and remaining problems. *Geologcal Bulletin of China* **28**, 1693–703.

Mo, X., Zhao, Z., Deng, J., Dong, G., Zhou, S., Guo, T. & Wang, L. 2003. Response of volcanism to the India-Asia collision. *Earth Science Frontiers* **10**, 135–48.

Pearce, J. A., Harris, N. B. & Tindle, A. G. 1984. Trace element discrimination diagrams for the tectonic interpretation of granitic rocks. *Journal of Petrology* **25**, 956–83.

Qi, X., Zeng, L., Meng, X., Xu, Z. & Li, T. 2008. Zircon SHRIMP U-Pb dating for Dala granite in the Tethyan Himalaya and its geological implication. *Acta Petrologica Sinica* **24**, 1501–8.

Söderlund, U., Patchett, P.J., Vervoort, J.D. & Isachsen, C.E. 2004. The ^{176}Lu decay constant determined by Lu–Hf and U–Pb isotope systematics of Precambrian mafic intrusions. *Earth and Planetary Science Letters* **219**, 311–24.

Sun, S. S. & McDonough, W. S. 1989. Chemical and isotopic systematics of oceanic basalts: implications for mantle composition and processes. In *Magmatism in the Ocean Basins* (eds A. D. Saunders & M. J. Norry), pp. 313–45. Geological Society of London, Special Publication no. 42.

Sylvester, P. J. 1998. Post-collisional strongly peraluminous granites. *Lithos* **45**, 29–44.

Wu, F., Li, X., Zheng, Y. & Gao, S. 2007. Lu-Hf isotopic systematics and their applications in petrology. *Acta Petrologica Sinica* **23**, 185–220.

Wu, F., Zhao, Z., Liu, X. & Ji, W. 2015. Himalayan leucogranite. *Acta Petrologica Sinica* **31**, 1–36.

Wu, Y. & Zheng, Y. 2004. Zircon genetic mineralogy research and interpretation of U-Pb age restriction. *Chinese Science Bulletin* **49**, 1589–91.

Wu, Z., Ye, P., Wu, Z. & Zhao, Z. 2014. LA-ICP-MS zircon U-Pb ages of tectonic-thermal events in the Yardoi dome of Tethys Himalayan belt. *Geological Bulletin of China* **33**, 595–605.

Xie, K., Zeng, L., Liu, J. & Gao, L. 2010. The tectonic implications of Dala adakitic granite in late Eocene, southern Tibet. *Acta Petrologica Sinica* **26**, 1016–26.

Yu, J., Zeng, L., Liu, J., Gao, L. & Xie, K. 2011. Early Miocene leucogranites in Dinggye area, southern Tibet: formation mechanism and tectonic implications. *Acta Petrologica Sinica* **27**, 1961–72.

Zeng, L., Asimow, P. D. & Saleeby, J. B. 2005. Coupling of anatectic reactions and dissolution of accessory phases and the Sr and Nd isotope systematics of anatectic melts from a metasedimentary source. *Geochimica et Cosmochimica Acta* **69**, 3671–82.

Zeng, L., Gao, L., Hou, K. & Tang, S. 2012. Late Permian mafic magmafism along the Tethyan Himalayan Belt, southern Tibet and tectonic implications. *Acta Petrologica Sinica* **28**, 1731–40.

Zeng, L., Gao, L. E., Tang, S., Hou, K., Guo, C. & Hu, G. 2015. Eocene magmatism in the Tethyan Himalaya, southern Tibet. In *Tectonics of the Himalaya* (eds S. Mukherjee, R. Carosi, P. A. Van der Beek, B. K. Mukherjee & D. M Robinson), pp. 287–316. Geological Society of London, Special Publication no. 412.

Zeng, L., Gao, L. E., Xie, K. & Liu-Zeng, J. 2011. Mid-Eocene high Sr/Y granites in the Northern Himalayan Gneiss Domes: melting thickened lower continental crust. *Earth and Planetary Science Letters* **303**, 251–66.

Zeng, L., Liu, J., Gao, L., Xie, K. & Wen, L. 2009. Crustal anatexis and its geological significance of Yalaxaingbo dome in early Oligocene, Southern Tibet. *Chinese Science Bull*etin **54**, 373–81.

https://doi.org/10.1017/S0016756817000966 Published online by Cambridge University Press

Zhang, H., Harris, N., Parrish, R., Zhang, L. & Zhao, Z. 2004. Zircon SHRIMP U-Pb dating for Kutui and Sajia leucogranite in the northern Himalayan Sajia dome and its geological implication. *Chinese Science Bulletin* **49**, 2090–4.

Zhang, H., Harris, N., Parrish, R., Zhang, L., Zhao, Z. & Li, D. 2005.Geochemistry of North Himalayan leucogranites: regional comparison, petrogenesis and tectonic implications. *Earth Science-Journal of China University of Geosciences* **30**, 275–88.

Zhang, J., Guo, L. & Zhang, B. 2007. Structure and kinematics of the Yalashangbo dome in the northern himalayan dome Belt, China. *Chinese Journal of Geology* **42**, 16–30.

Zhang, L., Ding, L., Yang, D., Xu, Q., Cai, F. & Liu, D. 2012. Origin of middle Miocene leucogranites and rhyolites on the Tibetan Plateau: constraints on the timing of crustal thickening and uplift of its northern boundary. *Chinese Science Bulletin* **57**, 511–24.

Zhao, Z., Zheng, Y. & Dai, L. 2013. Causes and nature of the magma origin region of inherited zircon in granite in continental collision orogenic belt. *Chinese Science Bulletin* **58**, 2285–9.

https://doi.org/10.1017/S0016756817000966 Published online by Cambridge University Press